Nonlocal thermal transport modeling using the thermal distributor

Ali Kefayati [1,*] Philip B. Allen [2,†] and Vasili Perebeinos [1,‡]

[1]*Department of Electrical Engineering, University at Buffalo, The State University of New York, Buffalo, New York 14260, USA*

[2]*Department of Physics and Astronomy, Stony Brook University, Stony Brook, New York 11794-3800, USA*

(Received 8 January 2022; revised 22 March 2022; accepted 20 May 2022; published 2 June 2022)

Thermal transport in a quasiballistic regime is determined not only by the local temperature $T(r)$ or its gradient $\nabla T(r)$ but also by the temperature distribution at neighboring points. For an accurate description of nonlocal effects on thermal transport, we employ the thermal distributor $\Theta(r, r')$, which provides the temperature response of the system at point r to the heat input at point r'. We determine the thermal distributors from the linearized Peierls-Boltzmann equation, both with and without the relaxation time approximation, and employ them to describe thermal transport in quasiballistic graphene devices.

DOI: 10.1103/PhysRevB.105.235402

I. INTRODUCTION

Advances in technology and experimental studies beyond microscale dimensions of materials require new insights into theoretical models that were developed initially based on continuum transport theories. The Peierls formulation of thermal transport in solids (the Peierls-Boltzmann equation, PBE [1]) is based on the quasiparticle picture of phonons. The temperature gradient ∇T enters the PBE as a driving force. At macroscopic scales and in steady state, the PBE leads to Fourier's law, $\vec{J} = -\kappa(T_0)\nabla T$, where $\kappa(T_0)$ is the thermal conductivity at the background temperature T_0 and $\vec{J}$ is the heat current density. Small variations of the temperature gradient are ignored. This is called the diffusive regime.

Early experiments on thermal transport in submicron devices [2–6] showed that the temperature gradient is not constant but varies on length scales shorter than or comparable to the mean free path (MFP) of phonons. Often, the analysis of experiment suggests a version of Fourier's law using an "effective thermal conductivity." The experiments indicate a nondiffusive regime, with a nonlocal relation between the heat current and temperature gradient. Fourier's law requires generalization, and Boltzmann's theory does this well [4,7–11]. The Boltzmann equation describes the evolution of the phonon distribution function $N_Q(r, t)$. When phonons are driven away from equilibrium by local power insertion, it is necessary to add a new term, $(dN_Q/dt)_{\text{ext}}$, describing the power $P_Q(r, t)$ added to the phonon mode Q. The local temperature $T(r, t) = T_0 + \Delta T(r, t)$ is an ultimate goal but is not needed to find the nonequilibrium distribution. The inserted power $P_Q(r, t)$ is enough to determine N_Q and the corresponding heat current $\vec{J}(r, t)$. The local temperature deviation $\Delta T(r, t)$ is an important measure of the behavior of the system, but Boltzmann's theory does not contain a definition of $\Delta T(r, t)$; it is necessary to choose a definition. The correct definition is the one in which $C\Delta T(r, t) = \Delta E(r, t)$, where $\Delta E(r, t)$ is the deviation of the total nonequilibrium phonon energy of the system when it is driven away from the equilibrium state at the background temperature T_0 and C is the specific heat. Unfortunately, when the Boltzmann scattering operator is approximated by the relaxation time approximation (RTA), an alternate and less physical definition is necessary to restore the energy conservation that is broken by RTA. In this paper, we find $\Delta T(r, t)$ by solving the linearized PBE (LPBE) using the full scattering operator and the correct definition and compare it with the RTA version.

Solving the PBE requires a matrix inversion, which is often avoided by using the relaxation time approximation,

$$\left(\frac{\partial N_Q}{\partial t}\right)^{\text{RTA}}_{\text{scatt}} = -\frac{N_Q(\vec{r}, t) - n_Q(T(\vec{r}, t))}{\tau_Q}. \tag{1}$$

Here $Q = (\vec{q}, s)$ labels phonon modes: $\vec{q}$ is the wave vector, and s is the branch index. The Bose-Einstein distribution $n_Q(T(\vec{r}, t))$ is evaluated at the local temperature $T(\vec{r}, t)$. The phonon relaxation rate $1/\tau_Q$ is evaluated using Fermi's golden rule for anharmonic three- phonon scatterings. It is also the diagonal part of the linearized scattering operator $\hat{S}^0$,

$$\left(\frac{\partial N_Q}{\partial t}\right)^{\text{LPBE}}_{\text{scatt}} = -\sum_{Q'} S^0_{QQ'}(N_{Q'} - n_{Q'}). \tag{2}$$

In this version labeled with a superscript 0, $1/\tau_Q = S^0_{QQ}$, the correctly linearized operator $\hat{S}^0$ is non-Hermitian. For numerical inversion, it is preferable instead to define [12]

$$N_Q(\vec{r}, t) \equiv n_Q(T(\vec{r}, t)) + n^0_Q(T_0)\left[n^0_Q(T_0) + 1\right]\phi_Q(\vec{r}, t), \tag{3}$$

$$\left(\frac{\partial N_Q}{\partial t}\right)^{\text{LPBE}}_{\text{scatt}} = -\sum_{Q'} S_{QQ'}\phi_{Q'}, \tag{4}$$

where $n^0_Q(T_0)$ is the Bose-Einstein distribution at equilibrium temperature T_0. Then the operator $\hat{S}$ is Hermitian, and the

*alikefay@buffalo.edu
†philip.allen@stonybrook.edu
‡vasilipe@buffalo.edu

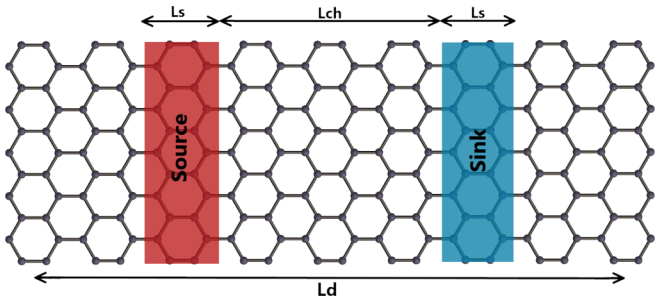

FIG. 1. Schematic of inhomogeneous external driving with periodic boundary conditions. The finite system has a length $L_d = 2L_s + 2L_{ch}$, which is repeated periodically, where L_{ch} is the channel length and L_s is the source/sink heat length. Thermal energy at rate P is added at the source and removed at the sink.

diagonal element is

$$S_{QQ} = n_Q^0(T_0)\left[n_Q^0(T_0) + 1\right]/\tau_Q. \tag{5}$$

The spatially homogeneous PBE driven by a constant ∇T has been solved by inversion of this Hermitian operator $\hat{S}$ [13–22]. For spatially inhomogeneous situations, the LPBE [in Fourier space $(\vec{k}, \eta)$ rather than coordinate space $(\vec{r}, t)$] requires much more difficult inversion of the non-Hermitian operator $S_{QQ'} + i(\vec{k}\cdot\vec{v}_Q - \eta)\delta_{QQ'}$, where $\vec{v}_Q$ is the velocity of the phonon mode Q. Difficult inversion is avoided by using the RTA $S_{QQ'} \to \delta_{QQ'} n_Q(n_Q + 1)/\tau_Q$ [23–26]. Recently, inversions with the correct scattering operator for inhomogeneous transport have been done [10,27].

In [8], the authors introduced a concept called thermal susceptibility, inspired by the definition of the electrical susceptibility. Thermal susceptibility relates the temperature deviation at $(\vec{r}, t)$ to the heat insertion at $(\vec{r}\,', t')$. This study aims to investigate the capability of the *thermal distributor* function Θ, which is a redefined version of the thermal susceptibility function,

$$\Theta(\vec{r} - \vec{r}\,', t - t') \equiv \frac{\delta T(\vec{r}, t)}{\delta P(\vec{r}\,', t')}, \tag{6}$$

for the analysis of nonlocal thermal transport. Thus, the temperature deviation is obtained,

$$\Delta T(\vec{r}, t) = \frac{1}{V}\int d\vec{r}\,' \int_{-\infty}^{t} dt' \Theta(\vec{r} - \vec{r}\,', t - t') P(\vec{r}\,', t'), \tag{7}$$

where V is the sample volume. In reciprocal space, $\Delta T(\vec{k}, \eta) = \Theta(\vec{k}, \eta) P(\vec{k}, \eta)$. We apply our analysis to graphene, as depicted in Fig. 1.

Because graphene is a two-dimensional crystal, the vectors $\vec{r}$ and $\vec{k}$ are two-dimensional. Because the heat source and sink are parallel to the y axis, the relevant wave vector is $\vec{k} = (k_x, 0)$. Heat current density $\vec{J}_{2D}$ has units of watts per meter; the more familiar unit in three dimensions is watts per square meter. Thermal conductivity in two dimensions has units of watts per kelvin; in order to compare it with three-dimensional (3D) results, it is conventional to choose the somewhat arbitrary "thickness" for graphene to be $h = 3.4$ Å. This paper uses 3D units for current density $J = J_{2D}/h$, input power $P = P_{2D}/h$, energy density $U = U_{2D}/h$, and specific heat $C = C_{2D}/h$. Then κ has the conventional units of watts per millikelvin, and Θ has units of cubic kilometers per watt.

The measured thermal conductivity of graphene (in 3D units) is reported to lie in the range of 2600 to 5300 W/mK at room temperature [28,29]. The theoretical thermal conductivity of pristine infinite-size graphene at room temperature is reported in the range of 2800–4300 W/mK [13,19,30]. In devices smaller than the mean free paths Λ_Q of important phonons, the measured heat current divided by an approximate measurement of temperature gradient gives an effective thermal conductivity κ_{eff} of smaller value. For phonons with bulk $\Lambda_Q = |v_{Qx}|\tau_Q$ ($\vec{v}_Q$ is the phonon group velocity) greater than device size L, the contribution to κ_{eff} is reduced from $C_Q|v_{Q,x}|\Lambda_Q$ to $C_Q|v_{Qx}|L$, where C_Q is the contribution of mode Q to the specific heat. We will describe this effect using the thermal distributor function [23].

II. FORMALISM

Under the assumptions of well-defined quasiparticles, the PBE in a crystalline solid is

$$\frac{dN_Q}{dt} = \left(\frac{\partial N_Q}{\partial t}\right)_{\text{drift}} + \left(\frac{\partial N_Q}{\partial t}\right)_{\text{scat}} + \left(\frac{\partial N_Q}{\partial t}\right)_{\text{ext}}. \tag{8}$$

The first term on the right-hand side of Eq. (8) is the change in N_Q caused by phonon drift in the distribution gradient:

$$\left(\frac{\partial N_Q}{\partial t}\right)_{\text{drift}} = -\vec{v_Q}\cdot\vec{\nabla}_{\vec{r}} N_Q, \tag{9}$$

where $\vec{\nabla}_{\vec{r}}$ is the spatial gradient. The second term in Eq. (8) contains all scattering processes in the crystal. The term from anharmonic three-phonon scatterings ($Q \to Q' + Q''$, $Q + Q' \to Q''$) can be found from Fermi's golden rule [31]:

$$\begin{aligned}\left(\frac{\partial N_Q}{\partial t}\right)_{\text{scat}} = \frac{\pi\hbar}{16N_q}\sum_{Q'Q''}|V_{QQ'Q''}|^2\frac{1}{2}\{&N_Q(N_{Q'}+1)(N_{Q''}+1)\\ &- (N_Q+1)N_{Q'}N_{Q''}\}\delta(\omega_Q - \omega_{Q'} - \omega_{Q''})\\ &+ \{N_Q N_{Q'}(N_{Q''}+1) - (N_Q+1)(N_{Q'}+1)N_{Q''}\}\\ &\times \delta(\omega_Q + \omega_{Q'} - \omega_{Q''}),\end{aligned} \tag{10}$$

where ω_Q is the phonon frequency and N_q is the number of wave vectors in the Brillouin zone [32]. $V_{QQ'Q''}$ is the matrix element of the three-phonon process, given by

$$\begin{aligned}V_{QQ'Q''} = \sum_{MLnml}\sum_{\alpha\beta\gamma}\frac{\epsilon_Q^{n\alpha}\epsilon_{Q'}^{m\beta}\epsilon_{Q''}^{l\gamma}}{\sqrt{M_c^3\omega_Q\omega_{Q'}\omega_{Q''}}}\Psi_{\alpha\beta\gamma}(0n, Mm, Ll)e^{i\boldsymbol{q}'\cdot\boldsymbol{R}_M}\\ \times e^{i\boldsymbol{q}''\cdot\boldsymbol{R}_L}\delta(q + q' + q'', G),\end{aligned} \tag{11}$$

where $\Psi_{\alpha\beta\gamma}(0n, Mm, Ll)$ is the third derivative of the crystal potential by displacements of atoms in positions (n, m, l) inside unit cells $(0, M, L)$. The supercell with index 0 is the central unit cell. $\epsilon_Q^{n\alpha}$ is the αth Cartesian component of the polarization vector of mode Q at atom n, and M_c is the mass of a carbon atom. The Kronecker delta ensures the conservation of the lattice momentum, where G is a reciprocal lattice vector. The local equilibrium phonon population $n_Q = n_Q(T(\vec{r}, t))$ depends implicitly on the space and time through its explicit

dependence on the temperature $T(\vec{r},t)$. For small deviations from equilibrium, we expand the phonon population N_Q as in Eq. (3) to first order in ϕ_Q. The anharmonic scattering matrix $\hat{S}$ [Eq. (4)] then has diagonal and off-diagonal elements,

$$\begin{aligned} S_{QQ} &= 1/\tau_Q = 2\pi\hbar \sum_{Q'Q''} |V_{QQ'Q''}|^2 \left\{ \frac{\left(n^0_Q+1\right)n^0_{Q'}n^0_{Q''}}{2}\delta(\omega_Q-\omega_{Q'}-\omega_{Q''}) + n^0_Q n^0_{Q'}\left(n^0_{Q''}+1\right)\delta(\omega_Q+\omega_{Q'}-\omega_{Q''})\right\}, \\ S_{QQ'} &= 2\pi\hbar \sum_{Q''} |V_{QQ'Q''}|^2 \left\{ n^0_Q n^0_{Q'}\left(n^0_{Q''}+1\right)\delta(\omega_Q+\omega_{Q'}-\omega_{Q''}) - \left(n^0_Q+1\right)^0_{Q'} n^0_{Q''}\delta(\omega_Q-\omega_{Q'}-\omega_{Q''}) \right. \\ &\quad \left. - n^0_Q\left(n^0_{Q'}+1\right)n^0_{Q''}\delta(\omega_Q-\omega_{Q'}+\omega_{Q''})\right\}. \end{aligned} \tag{12}$$

This version of the scattering matrix is real symmetric ($S_{QQ'} = S_{Q'Q}$), i.e., Hermitian. Each collision conserves phonon energy, which is ensured by

$$S_{QQ}\omega_Q + \sum_{Q',Q'\neq Q} S_{QQ'}\omega_{Q'} = 0, \text{ or } \hat{S}|\omega\rangle = 0. \tag{13}$$

The mode frequency $\omega_Q = \langle Q|\omega\rangle$ is an eigenvector, in fact, the *only* "null eigenvector," of the linearized Hermitian scattering operator $S_{QQ'} = \langle Q|\hat{S}|Q'\rangle$.

The last term in Eq. (8) models external heat sources and sinks. The form is usually [33,34]

$$\left(\frac{\partial N_Q}{\partial t}\right)_{\text{ext}} = \frac{P_Q(\vec{r},t)}{C}\frac{dn_Q}{dT}. \tag{14}$$

The heat source/sink P, its geometry $(\vec{r},t)$, and its spectral distribution Q determine whether the heat transport is quasiballistic or diffusive. We use the simplest version where $P_Q = P$ is independent of Q [8,34–36],

$$\left(\frac{\partial N_Q}{\partial t}\right)_{\text{ext}} = \frac{P}{C}\frac{dn_Q}{dT}, \tag{15}$$

where P is the heat power added per unit volume of the system. Each mode gets the same boost ΔT from $P(\vec{r},t)$. Detailed knowledge of the source and sink would cause a Q dependence of P [23,37], but lacking this knowledge, $P_Q = P$ is a sensible guess.

In vector-space notation, the LPBE, Eq. (8), is

$$\begin{aligned} \frac{\partial}{\partial t}[|n\rangle + |n^0(n^0+1)\phi\rangle] &= -\vec{v}_Q\vec{\nabla}_{\vec{r}}[|n\rangle + |n^0(n^0+1)\phi\rangle] \\ &\quad - \hat{S}|\phi\rangle + \frac{P(\vec{r},t)}{C}|\frac{dn}{dT}\rangle. \end{aligned} \tag{16}$$

In this notation, the kets (like $|n\rangle$) are vectors in the space of phonon modes, with components $\langle Q|n\rangle = n_Q$. The solution $\phi_Q(\vec{r},t)$ is found from its Fourier $(\vec{k},\eta)$ representation,

$$\phi_Q(\vec{r},t) = \frac{1}{2\pi}\int_{-\infty}^{\infty} d\eta e^{-i\eta t}\sum_{\vec{k}} e^{i\vec{k}\cdot\vec{r}}\phi(\vec{k},\eta). \tag{17}$$

The temperature deviation $\Delta T(\vec{r},t)$ and the power input $P(\vec{r},t)$ are also transformed to Fourier space. To simplify the algebra, we define a vector $|X\rangle$ and an operator $\hat{W}$:

$$|X\rangle \equiv |n^0(n^0+1)\hbar\omega\rangle, \tag{18}$$

$$\hat{W} \equiv \hat{S} + i(\vec{k}\cdot\hat{\vec{v}} - \eta\hat{1})\hat{n}^0(\hat{n}^0+\hat{1}), \tag{19}$$

where $\hat{\vec{v}}$ and $\hat{n}^0$ are diagonal in Q space [i.e., $\langle Q|\hat{n}^0|Q'\rangle = n^0_Q\delta(Q,Q') = \langle Q|n^0\rangle\delta(Q,Q')$]. The LPBE in Fourier space is

$$\begin{aligned} \hat{W}|\phi\rangle = \frac{1}{k_B T^2}\Big[&- i(\vec{k}\cdot\hat{\vec{v}} - \eta\hat{1})\Delta T(\vec{k},\eta) \\ &+ \frac{P(\vec{k},\eta)}{C}\hat{1}\Big]|X\rangle. \end{aligned} \tag{20}$$

A. Thermal distributor

By inverting the matrix $\hat{W}$, the distribution $|\phi(\vec{k},\eta)\rangle$ is found. The nonequilibrium energy density $\Delta U(\vec{r},t)$ is the total local energy density minus the energy density of the system equilibrated at the local temperature $T(\vec{r},t) = T_0 + \Delta T(\vec{r},t)$. Its Fourier version is

$$\begin{aligned} \Delta U(\vec{k},\eta) &= \frac{1}{V}\langle X|\phi\rangle \\ &= \frac{1}{Vk_BT^2}\Big[\langle X|\hat{W}^{-1}|[-i(\vec{k}\cdot\vec{v}-\eta)]X\rangle\Delta T(\vec{k},\eta) \\ &\quad + \langle X|\hat{W}^{-1}|X\rangle\frac{P(\vec{k},\eta)}{C}\Big]. \end{aligned} \tag{21}$$

After transients have died out, the local equilibrium part $|n(T(\vec{r},t))\rangle$ of the distribution contains all the heat, and the deviation $|n_0(n_0+1)\phi\rangle$ contains no net heat. This is a result of Boltzmann's H theorem, which says that before a steady state is reached, collisions increase entropy. The steady state occurs when entropy is maximum, which happens when the distribution evolves to a Bose function $|n(T(\vec{r},t))\rangle$ that contains all the heat energy [8]. Therefore, $\Delta U(\vec{k},\eta) = 0$, and the thermal distributor function $\Theta(\vec{k},\eta)$, defined in Eq. (7), can be calculated from Eq. (21) as

$$\begin{aligned} \Theta(\vec{k},\eta) &= \frac{\Delta T(\vec{k},\eta)}{P(\vec{k},\eta)} \\ &= \frac{1}{C}\frac{\langle X|\hat{W}^{-1}|X\rangle}{\langle X|\hat{W}^{-1}|i(\vec{k}\cdot\vec{v}-\eta)X\rangle}. \end{aligned} \tag{22}$$

This is the linear relation that gives the local temperature deviation caused by the external heat power input P.

B. Thermal conductivity

The thermal current, using Eq. (20), is

$$\vec{J}(\vec{k},\eta) = \sum_Q \hbar\omega_Q \vec{v}_Q n_Q^0\left(n_Q^0+1\right)\phi_Q(\vec{k},\omega) = \frac{1}{V}\langle \vec{v}X|\phi\rangle$$

$$= \frac{1}{Vk_BT^2}\left[\langle \vec{v}X|\hat{W}^{-1}|[-i(\vec{k}\cdot\vec{v}-\eta)]X\rangle \Delta T(\vec{k},\eta) + \langle \vec{v}X|\hat{W}^{-1}|X\rangle \frac{P(\vec{k},\eta)}{C}\right]. \quad (23)$$

In Fourier space, Fourier's law reads $\vec{J}(\vec{k},\eta) = -i\vec{k}\kappa(\vec{k},\eta)\Delta T(\vec{k},\eta)$, and the thermal conductivity according to Eqs. (22) and (23) is

$$\kappa(\vec{k},\eta) = \frac{i\vec{k}\vec{J}(\vec{k},\eta)}{k^2\Delta T(\vec{k},\eta)} = \frac{1}{k^2Vk_BT^2}\left[\langle i\vec{k}\cdot\vec{v}X|\hat{W}^{-1}|[-i(\vec{k}\cdot\vec{v}-\eta)]X\rangle + \langle i\vec{k}\cdot\vec{v}X|\hat{W}^{-1}|X\rangle \frac{\langle X|\hat{W}^{-1}|i(\vec{k}\cdot\vec{v}-\eta)X\rangle}{\langle X|\hat{W}^{-1}|X\rangle}\right]. \quad (24)$$

Using Eqs. (18) and (19), we can write $|i(\vec{k}\cdot\vec{v}-\eta)X\rangle$ as $(\hat{W}-\hat{S})|\hbar\omega\rangle$. Using time-reversal symmetry, $\hat{S}|\hbar\omega\rangle = 0$, and $\langle X|\hbar\omega\rangle = CVk_BT^2$, we can simplify Eq. (24) to

$$\kappa(\vec{k},\eta) = \frac{C}{k^2}\left[\frac{\langle i\vec{k}\vec{v}X|\hat{W}^{-1}|X\rangle}{\langle X|\hat{W}^{-1}|X\rangle}\right]. \quad (25)$$

By comparing Eq. (25) with Eq. (22), the relation between the thermal distributor and thermal conductivity is [8]

$$\kappa(\vec{k},\eta) = \frac{1}{k^2}\left(\frac{1}{\Theta(\vec{k},\eta)} + iC\eta\right). \quad (26)$$

Recently, it was shown [9,10] that unless P_Q is independent of mode Q, the response function $\kappa(\vec{k},\eta)$ is not a full description of nonlocal thermal heat transport. The current in Fourier space has the more general form $J(\vec{k},\eta) = -\kappa(\vec{k},\eta)\nabla T(\vec{k},\eta) + B(\vec{k},\eta)$, where B vanishes if P is independent of Q. We agree and find that the thermal distributor also needs modification. Specifically, the temperature in Fourier space takes the form $\Delta T(\vec{k},\eta) = \Theta(\vec{k},\eta)P(\vec{k},\eta) + G(\vec{k},\eta)$, where $P(\vec{k},\eta)$ is the mode average of $P_Q(\vec{k},\eta)$ and $G(\vec{K},\eta)$ vanishes if P is independent of mode Q. We simplify the issue by choosing P to be independent of Q.

C. One-dimensional heat transport in the dc limit

We now focus on the dc heat transport along the x direction of graphene. Therefore, $\eta = 0$, and the wave vector $\vec{k}$ and velocity $\vec{v}_Q$ have only one relevant component each, $k_x \equiv k$ and $v_{Qx} \equiv v_Q$. The thermal distributor simplifies to

$$\Theta_{\rm LPBE}(k) = \frac{1}{C}\frac{\langle X|\hat{W}^{-1}|X\rangle}{\langle X|\hat{W}^{-1}|ikvX\rangle}. \quad (27)$$

We label it LPBE because it is obtained from the linear PBE, Eq. (20), and we want to distinguish it from the RTA version of the PBE. The local temperature $\Delta T(\vec{r})$ appearing in the LPBE, Eq. (21), is defined by the statement that the local equilibrium distribution $n_Q(T(\vec{r}))$ carries all the heat, and the deviation $N_Q - n_Q(T(\vec{r}))$ carries no heat; $\Delta U(\vec{r})$ in Eq. (21) is zero. How is $\Delta T(\vec{r})$ defined in RTA? It is a peculiar fact of the RTA that an alternative definition of $\Delta T(\vec{r})$ is preferable, namely,

$$\left(\frac{\partial U}{\partial t}\right)^{\rm RTA}_{\rm scat} = \sum_Q \hbar\omega_Q\left(\frac{\partial N_Q}{\partial t}\right)^{\rm RTA}_{\rm scat} = 0 = -\sum_Q \hbar\omega_Q \frac{N_Q - n_Q(T(\vec{r},t))}{\tau_Q}. \quad (28)$$

This option is known to work better than the alternative of setting ΔU to zero [8]. The RTA result for the thermal distributor is then

$$\Theta_{\rm RTA}(k) = \frac{1}{C}\frac{\sum_Q \frac{C_Q\Gamma_Q^2}{\Gamma_Q^2+(kv_Q)^2}}{\sum_Q \frac{C_Q\Gamma_Q(kv_{xQ})^2}{\Gamma_Q^2+(kv_Q)^2}}, \quad (29)$$

where $\Gamma_Q = 1/\tau_Q$.

III. RESULTS AND DISCUSSION

Quasiparticle heat transport in solids can be roughly categorized into three regimes: ballistic, quasiballistic, and diffusive. In the diffusive regime, where Fourier's law applies, the channel length of the heat conductors is much longer than the MFPs; phonons experience multiple scattering events, so that a local equilibrium is established, with a temperature gradient that is constant everywhere except in the small region close to heat sources and sinks. Thermal transport is ballistic when the channel length is comparable to or less than phonon MFPs. In this case, thermal energy is mainly dissipated near the heat sources. The temperature gradient becomes thermally inhomogeneous, and heat current has a nonlocal relation to temperature. When the channel length is similar to the averaged phonon MFP, some phonons travel ballistically, and others travel diffusely; heat transfer is "quasiballistic." The wide range of phonon MFPs in graphene [38] makes it hard to differentiate transport regimes. Moreover, the heat transport regime in a given device is temperature dependent since the phonon MFPs depend on temperature.

The thermal distributor $\Theta(\vec{r})$, Eq. (6), simplifies the description of heat transport in different regimes. The spatial variation of temperature is given by

$$T(\vec{r}) = \sum_{\vec{k}} T(\vec{k})e^{i\vec{k}\cdot\vec{r}} = \sum_{\vec{k}} \Theta(\vec{k})P(\vec{k})e^{i\vec{k}\cdot\vec{r}}. \quad (30)$$

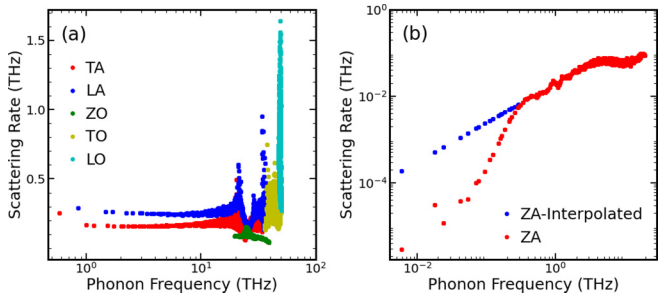

FIG. 2. Anharmonic three-phonon scattering rates for graphene at room temperature are shown in (a) on a linear scale for transverse acoustic (TA), longitudinal acoustic (LA), out-of-plane optical (ZO), transverse optical (TO), and longitudinal optical (LO) phonon modes; (b) shows the scattering rates of flexural mode (ZA) on a log scale. The blue circles show linear interpolation of the ZA scattering rate for frequencies below 0.3 THz, see text.

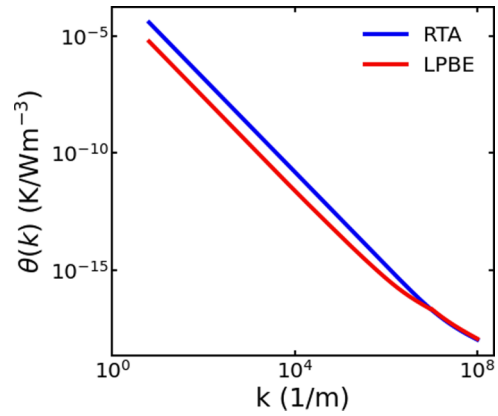

FIG. 3. Fourier transform of the thermal distributor as a function of momentum k in graphene using the RTA and LPBE approaches. The small-k limit corresponds to large distances from the input of the heat source such that thermal transport is diffusive and $\Theta(k)$ diverges.

The Fourier transform $\Theta(\vec{k})$ is related to the nonlocal generalization of the bulk thermal conductivity $\kappa_{\text{bulk}} = \lim_{\vec{k}\to 0}\kappa(\vec{k})$ by Eq. (26). First, we calculate LPBE and RTA versions of $\Theta(\vec{k})$ of graphene from Eqs. (27) and (29), using the modified Tersoff potential with the parameters given in Ref. [39], to model the crystal potential. The scattering rates are shown in Fig. 2 at $T = 300$ K.

Note that there are numerical challenges in calculating the scattering rates of phonons using the Gaussian broadening [40]. Following Refs. [13,31], we apply linear interpolation of the ZA scattering rates with phonon energy, as shown by the blue circles for phonon energies below 0.3 THz in Fig. 2(b). This linear scaling is explained by noting that the bending energy is given by $E_b = \int d^2r\kappa_b/(2R^2)$, where $\kappa_b = 2.1$ eV [41] is the bending stiffness and R is the radius of curvature given by $1/R = d^2z/dx^2$. Applying the Bloch theorem for a discrete atomic model with a lattice constant a, one can show that bending energy for mode q is given by $E_b = 8\kappa_b A_c z_q^2 \sin^4(qa/2)/a^4 \approx A_c\kappa_b z_q^2 q^4/2$, where A_c is the area per atom. By comparing it to the harmonic oscillator potential energy $m\omega_q^2 z_q^2/2$, one can obtain the expected result for flexural phonon frequency: $\omega_q = q^2\sqrt{\kappa_b A_c/m}$. The third-order anharmonicity can be introduced by coupling the ZA mode to an LA mode by modifying the bending stiffness $\kappa_b = \kappa_{b0} - \alpha_b(x_{i+1} - x_{i-1})$. After applying the Bloch theorem, the third-order anharmonic potential for mode q in the small-q limit becomes $H_3 = \sum_{q_1} i\alpha_b A_c z_q z_{q_1} x_{-q-q_1} q^2 q_1^2 (q + q_1)a$. Using second-quantized amplitudes for the phonon displacements z_q and x_q, one can show that $V_{qq_1} \sim q^2 q_1^2 (q + q_1)(\omega_q^{\text{ZA}}\omega_{q_1}^{\text{ZA}}\omega_{q+q_1}^{\text{LA}})^{-1/2}$. The q-ZA phonon scattering with the q_1-ZA phonon into a $(q + q_1)$-LA phonon has a rate of $1/\tau_q^{\text{ZA}} \sim \sum_{q_1} |V_{q,q_1}|^2 n_{q_1}^{0,\text{ZA}} n_{q+q_1}^{0,\text{LA}} \delta(\omega_q^{\text{ZA}} + \omega_{q_1}^{\text{ZA}} - \omega_{q+q_1}^{\text{LA}})$. The δ function ensures that $q_1 \sim v_s\sqrt{m/(\kappa_b A_c)}$, where v_s is the sound velocity. Therefore, the interpolation function $1/\tau_q^{\text{ZA}} \sim q^2 \sim \omega_q^{\text{ZA}}$ used in Fig. 2(b) can be justified.

Figure 3 shows the calculated $\Theta(k)$ for graphene using the LPBE and RTA. The width of the sample is much broader than the MFP; this allows a one-dimensional treatment. The spatial variation $\vec{r} = (x, 0)$ is only along $\hat{x}$, parallel to the channel, so the spatial Fourier variable is $\vec{k} = (k, 0)$. The spatial resolution of $T(x)$ at small distances x requires values of $\Theta(k)$ at correspondingly large $k \sim 2\pi/x$ [see Eq. (30)]. The range of k in Fig. 3 corresponds to distances from a few nanometers to a meter-long channel length. A lower limit of the length scale is imposed by the validity of the quasiparticle picture of phonons used in the PBE formalism [26]. Note that the thermal distributor diverges for both LPBE and RTA solutions when $k \to 0$. According to Eq. (26), for a finite thermal conductivity in a diffusive regime, $\Theta(k)$ must diverge in the $k \to 0$ limit as $\Theta(k) \sim \frac{1}{k^2}$. Curve fitting shows that the calculated $\Theta(k)$ for both versions agrees with $\frac{1}{k^2}$ very accurately in the small-k limit, namely,

$$\Theta_{\text{LPBE}}(k) = \frac{2.4\times 10^{-4}\ \text{km/W}}{k^2},$$
$$\Theta_{\text{RTA}}(k) = \frac{1.51\times 10^{-3}\ \text{km/W}}{k^2}. \tag{31}$$

Using Eq. (26), this corresponds to bulk thermal conductivities of 4145 and 662 W/mK for LPBE and RTA, respectively. The large discrepancy between LPBE and RTA values of thermal conductivities in graphene was noticed previously [13].

The thermal conductivities evaluated according to Eq. (25) for LPBE and Eqs. (26) and (29) for RTA are shown in Fig. 4.

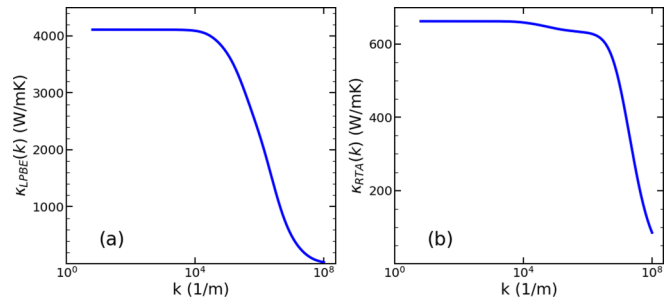

FIG. 4. Thermal conductivity using (a) the LPBE and (b) RTA approaches.

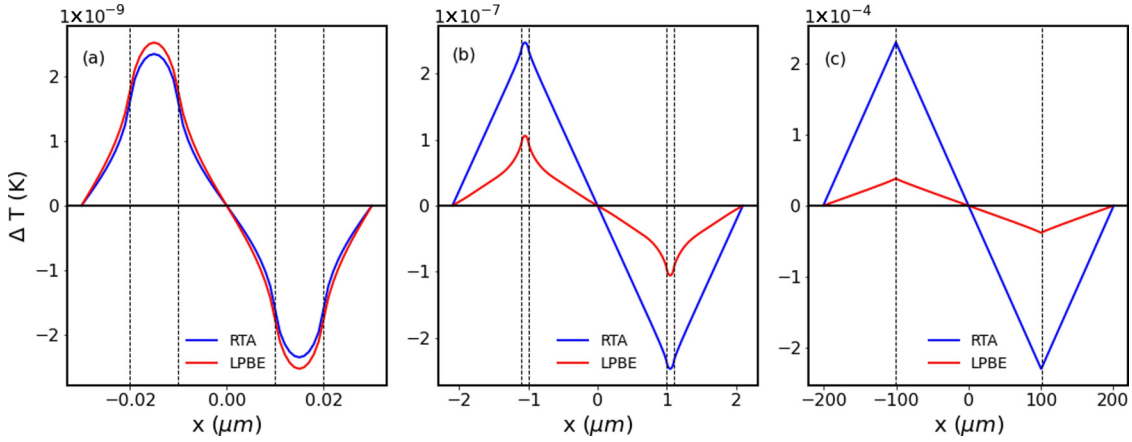

FIG. 5. Temperature variation $\Delta T(x) = T(x) - T_0$ at $T_0 = 300$ K for three different values of the channel length: (a) $L_{\rm ch} = 20$ nm, (b) $L_{\rm ch} = 2\ \mu$m, and (c) $L_{\rm ch} = 200\ \mu$m. The source/sink lengths are $L_{\rm s} = 10$ nm, 100 nm, and 1 μm in (a), (b), and (c), respectively. Input power $P(x) = P_0 = (1\text{W/m}^2)/h = 2.94 \times 10^9 \text{W/m}^3$ is applied in all calculations. The effective thermal conductivities are given in Table I.

The sharp falloff of the thermal conductivity in Fig. 4 indicates the ballistic-to-diffusive crossover; it happens at larger k and, therefore, smaller characteristic lengths in the RTA treatment than in the correct LPBE treatment.

Now we discuss thermal conduction in the geometry of Fig. 1 using the PBE to evaluate the thermal distributor. We can calculate the temperature profile for any pattern of heat input and removal from this response function, provided the graphene sample has one-dimensional periodicity. Energy conservation requires $dJ/dx = -P(x)$. Steady state ($\eta = 0$) requires equal external heat addition and removal. $L_{\rm ch}$ is the length of the channel between the two heat reservoirs, the source and sink, each of length $L_{\rm s}$. For simplicity, our heat input has odd symmetry $[P(-x) = -P(x)]$ around $x = 0$, so J is even in x. The period of the supercell is $L_d = 2(L_{\rm ch} + L_{\rm s})$, which determines the shortest nonzero wave vector, i.e., $k_{\rm min} = 2\pi/L_d$. A large L_d value allows a fine Fourier mesh to describe nanoscale physics, such as the ballistic-to-diffusive crossover. Our reservoirs are ideal thermal baths, with zero interfacial thermal resistance between the channel and reservoirs. Note that experimental thermal conductivity measurements are often done using periodic structures such as periodic metallic gratings or transient thermal gratings [42,43]. Our periodic geometry in Fig. 1 works for both periodic structures and single-channel devices. In the latter case, it is necessary to make $L_{\rm s}$ larger than phonon MFPs.

Figure 1 shows how heat insertion and removal $P(x)$ are distributed uniformly (with magnitude P_0) over lengths $L_{\rm s}$ on either side of the sample (or channel) of length $L_{\rm ch}$. Energy conservation $dJ/dx = P$ then gives heat current density $J = P_0 L_{\rm s}/2$ in the channels. Figure 5 shows the resulting ΔT profiles in three devices with channel lengths spanning from ballistic to diffusive regimes. In the ballistic device [Fig. 5(a)], both $\Theta_{\rm RTA}$ and $\Theta_{\rm LPBE}$ predict similar values for temperature profiles in the channel and in the source/sink reservoirs. This behavior can be understood from the two thermal distributors being similar in magnitude in the large-k limit, as shown in Fig. 3. The temperature profile in Fig. 5(a) clearly shows the source regions are hotter than the channel, which is a characteristic of nondiffusive thermal transport [33,34,44]. The long MFP phonons (ZA phonons) dissipate the thermal energy in the source regions while flying in the channel ballistically. As a result, the temperature is higher in the heat region. This observation manifests the nonlocal effect.

For the larger channel lengths in Figs. 5(b) and 5(c), RTA predictions for the temperature are significantly higher than LPBE predictions, in agreement with Fig. 3, which shows that at smaller k (corresponding to larger distances) $\Theta_{\rm RTA}$ is greater than $\Theta_{\rm LPBE}(k)$. In the quasiballistic regime in Fig. 5(b), there is significant nonlinearity near the heat source/sink. Although in this regime both long and short MFP phonons contribute to thermal transport, the share of thermal energy carried by short MFP phonons is almost negligible.

Nonlocal heat transport is often described by an effective thermal conductivity $\kappa_{\rm eff}$. The definition varies depending on the experiment. For example, experimental studies such as those on time-domain thermoreflectance [45] measure the transient temperature response to a heat pulse. This can be used to extract $\kappa_{\rm eff}$ [42]. Many theoretical studies have also applied a similar procedure.

TABLE I. Effective thermal conductivities computed from three definitions for the cases shown in Fig. 5. The subscript mp means current density divided by the midpoint temperature gradient; min means the current divided by maximum ΔT per half supercell length, and ch means current divided by the temperature difference at the channel edges per channel length. The current density J_0 is the constant value in the channel.

LPBE	Definition	Fig. 5(a)	Fig. 5(b)	Fig. 5(c)
$\kappa_{\rm eff,mp}$	$\frac{J_0}{(dT/dx)_{x=0}}$	118	2463	4035
$\kappa_{\rm eff,min}$	$\frac{J_0}{\Delta T_{\rm max}/(L_{\rm ch}+L_{\rm s})}$	87	1460	3854
$\kappa_{\rm eff,ch}$	$\frac{J_0}{\Delta T_{\rm ch}/L_{\rm ch}}$	124	1565	3860
RTA	Definition	Fig. 5(a)	Fig. 5(b)	Fig. 5(c)
$\kappa_{\rm eff,mp}$	$\frac{J_0}{(dT/dx)_{x=0}}$	139	633	658
$\kappa_{\rm eff,min}$	$\frac{J_0}{\Delta T_{\rm max}/(L_{\rm ch}+L_{\rm s})}$	85	617	656
$\kappa_{\rm eff,ch}$	$\frac{J_0}{\Delta T_{\rm ch}/L_{\rm ch}}$	116	616	654

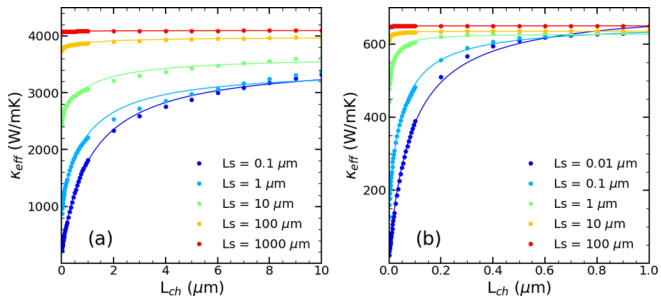

FIG. 6. Effective midpoint thermal conductivity at 300 K versus channel length calculated from the PBE and the geometry of Fig. 1 for different source lengths: (a) LPBE and (b) RTA solutions. For $L_s \leqslant 100$ μm ($L_s \leqslant 10$ μm) the transition from ballistic or quasiballistic to diffusive can be observed in LPBE (RTA) solutions. For $L_s > 100$ μm ($L_s > 10$ μm) the thermal transport is always in the diffusive regime for the LPBE (RTA) solution regardless of the source length. The solid curves are best fits to $\kappa_{\mathrm{eff,a}}$ in Eq. (32).

For our steady-state thermal transport computations, there are three sensible definitions of κ_{eff}, shown in Table I. The first of these defines κ_{eff} by applying Fourier's law in the middle of the channel where the curvature of $\Delta T(x)$ is zero. This resembles Fourier's law in thermally homogeneous structures. We note that in the fully diffusive regime, when both L_s and L_{ch} are larger than the MFPs, the $\kappa_{\mathrm{eff,mp}}$ and $\kappa_{\mathrm{eff,ch}}$ values coincide, and the temperature drop in the channel is $\Delta T_{\mathrm{ch}} = J_0 L_{\mathrm{ch}}/\kappa_{\mathrm{eff,mp}}$. In this limit, the temperature drop under the contact is equal to $J_0 L_s/(4\kappa_{\mathrm{eff,mp}})$ because current $J(x)$ varies linearly with distance from the middle of the contact. Therefore, the maximum temperature variation across the unit cell equals $\Delta T_{\max} = \Delta T_{\mathrm{ch}} + J_0 L_s/(2\kappa_{\mathrm{eff,mp}})$, and effective thermal conductivity $\kappa_{\mathrm{eff,min}} = J_0(L_{\mathrm{ch}} + L_s)/\Delta T_{\max} = \kappa_{\mathrm{eff,mp}}(L_{\mathrm{ch}} + L_s)/(L_{\mathrm{ch}} + L_s/2)$. As can be seen from Table I, the device geometry in Fig. 5(c) approaches the diffusive limit. However, one should note the fully diffusive limit relationship between $\kappa_{\mathrm{eff,min}}$ and $\kappa_{\mathrm{eff,mp}}$ is not realized in the devices we considered.

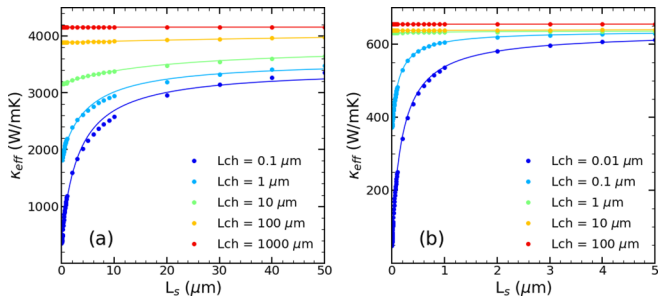

FIG. 7. Effective midpoint thermal conductivity at 300 K versus source length calculated for different channel lengths: (a) LPBE and (b) RTA solutions. For $L_{\mathrm{ch}} \leqslant 100$ μm ($L_{\mathrm{ch}} \leqslant 10$ μm), the transition from ballistic or quasiballistic to diffusive can be observed in the LPBE (RTA) solution. For $L_{\mathrm{ch}} > 100$ μm ($L_{\mathrm{ch}} > 10$ μm) the thermal transport is always in the diffusive regime for the LPBE (RTA) solution regardless of the source length. The solid curves are best fits to $\kappa_{\mathrm{eff,b}}$ in Eq. (33).

The $\kappa_{\mathrm{eff,mp}}$ definition is plotted in Figs. 6 and 7 for both LPBE and RTA versions of the thermal distributor as a function of the source length and channel length, respectively. When the chosen length L_{ch} in Fig. 6 (or L_s in Fig. 7) has a value less than the diffusive length scale ($\sim$1–3 μm for LPBE and $\sim$100–200 nm for RTA), $\kappa_{\mathrm{eff,mp}}$ decreases with decreasing periodicity due to suppression of the ballistic phonon contribution to the heat transport. At large values of L_{ch}, thermal conductivity saturates and approaches the diffusive limit when both L_{ch} and L_s are large.

Similarly, Fig. 7 shows that $\kappa_{\mathrm{eff,mp}}$ saturates with increasing L_s and reaches the diffusive limit value at large L_{ch}. For small L_{ch} values, the $\kappa_{\mathrm{eff,mp}}$ dependence on L_s shows ballistic-to-diffusive crossover as in Fig. 6. Those dependences happen because of superposing the interaction of ballistic phonons in the ballistic channels and recovery of diffusivelike thermal transport. This phenomenon shows the deterministic role of the geometry of the heat source and was already observed experimentally [43,46].

To quantify our results in Figs. 6 and 7, we fit our $\kappa_{\mathrm{eff,mp}}$ to the phenomenological ballistic-to-diffusive crossover equations used to describe electrical transport [47]:

$$\kappa_{\mathrm{eff,a}} = \kappa_0 + (\kappa_{\mathrm{dif}} - \kappa_0)\frac{L_{\mathrm{ch}}}{L_{\mathrm{ch}} + \lambda}, \tag{32}$$

$$\kappa_{\mathrm{eff,b}} = \kappa_0 + (\kappa_{\mathrm{dif}} - \kappa_0)\frac{L_s}{L_s + \lambda}, \tag{33}$$

where κ_{dif} is thermal conductivity in the diffusive regime. From the best fits, we find a characteristic length scale $\lambda \sim 1$ μm ($\sim$90 nm) for the LPBE (RTA) solution using fits of $\kappa_{\mathrm{eff,a}}$ versus L_{ch} and $\lambda \sim 3$ μm ($\sim$200 nm) for the LPBE (RTA) solution using fits of $\kappa_{\mathrm{eff,b}}$ versus L_s. The value of κ_0 approaches zero only when both L_s and L_{ch} are small, as discussed above. Those estimates for the characteristic crossover length scales are consistent with the k dependences of thermal conductivity in Fig. 4. Using a characteristic value of k_0, when thermal conductivity drops by a factor of 2 in Fig. 4, we find $2\pi/k_0 \sim 5$ μm for LPBE and $2\pi/k_0 \sim 300$ nm for RTA. Finally, we can estimate an average phonon MFP using the standard expression for thermal conductivity in two dimensions: $\kappa = Cv\lambda_{\mathrm{ph}}/2$, where the heat capacity is $C \times h = 4.5 \times 10^{-4}$ J/km^2 (calculated at $T = 300$ K) and v is an averaged phonon velocity. Using the velocity of the ZA parabolic band at room temperature $v \approx 10$ km/s, we obtain $\lambda_{\mathrm{ph}} = 625$ nm for LPBE and $\lambda_{\mathrm{ph}} = 100$ nm for RTA, consistent with the above estimates for the diffusive-to-ballistic crossover length scales.

IV. CONCLUSIONS

Steady microscale addition and removal of heat energy, together with a scattering of heat carriers, leads to carrier distributions N centered around local equilibrium n with a local temperature $T(x)$. The thermal distributor $\Theta(k)$ contains all relevant information about thermal transport in all the regimes. By computing the thermal distributor $\Theta(k)$ of graphene from the PBE with correct inversion using the full scattering operator, we investigated thermal transport at submicron length scales. At long length scales, heat transport occurs with constant temperature gradients. Nonlocal effects

(where ∇T varies with x) are seen at length scales of the order of or less than the mean free paths of phonons. The details of the geometrical structure of the device and heat sources and sinks cause the inhomogeneous temperature profile $T(x)$. The long-wavelength phonons are forcefully scattered in the source and sink regions while flying the channel without appreciable scatterings with other phonons. This causes local $\Delta T(x)$ to be higher near the source/sink. This is often ascribed to the suppression of heat transport by phonons with long mean free paths. The RTA contains these effects but, especially in graphene, overestimates the temperature inhomogeneity needed to drive a heat current.

ACKNOWLEDGMENTS

We acknowledge support from the Vice President for Research and Economic Development (VPRED), SUNY Research Seed Grant Program, and the Center for Computational Research at the University at Buffalo [48].

[1] R. Peierls, Zur kinetischen Theorie der Wärmeleitung in Kristallen, Ann. Phys. (Berlin, Ger.) **395**, 1055 (1929).
[2] S. Simons, The Boltzmann equation for a bounded medium I. General theory, Philos. Trans. R. Soc. London, Ser. A **253**, 137 (1960).
[3] Y. Levinson, Nonlocal phonon heat transfer, Solid State Commun. **36**, 73 (1980).
[4] G. D. Mahan and F. Claro, Nonlocal theory of thermal conductivity, Phys. Rev. B **38**, 1963 (1988).
[5] A. Majumdar, Microscale heat conduction in dielectric thin films, ASME J. Heat Transfer **115**, 7 (1993).
[6] G. Chen, *Nanoscale Energy Transport and Conversion: A Parallel Treatment of Electrons, Molecules, Phonons, and Photons* (Oxford University Press, Oxford, 2005).
[7] J. Ordonez-Miranda, R. Yang, and J. Alvarado-Gil, A constitutive equation for nano-to-macro-scale heat conduction based on the Boltzmann transport equation, J. Appl. Phys. **109**, 084319 (2011).
[8] P. B. Allen and V. Perebeinos, Temperature in a Peierls-Boltzmann treatment of nonlocal phonon heat transport, Phys. Rev. B **98**, 085427 (2018).
[9] C. Hua, L. Lindsay, X. Chen, and A. J. Minnich, Generalized Fourier's law for nondiffusive thermal transport: Theory and experiment, Phys. Rev. B **100**, 085203 (2019).
[10] C. Hua and L. Lindsay, Space-time dependent thermal conductivity in nonlocal thermal transport, Phys. Rev. B **102**, 104310 (2020).
[11] M. Simoncelli, N. Marzari, and A. Cepellotti, Generalization of Fourier's Law into Viscous Heat Equations, Phys. Rev. X **10**, 011019 (2020).
[12] G. P. Srivastava, *The Physics of Phonons* (Routledge, Taylor and Francis Group, New York, NY, 1990).
[13] L. Lindsay, W. Li, J. Carrete, N. Mingo, D. A. Broido, and T. L. Reinecke, Phonon thermal transport in strained and unstrained graphene from first principles, Phys. Rev. B **89**, 155426 (2014).
[14] L. Lindsay, First principles Peierls-Boltzmann phonon thermal transport: A topical review, Nanoscale Microscale Thermophys. Eng. **20**, 67 (2016).
[15] A. J. H. McGaughey, A. Jain, H.-Y. Kim, and B. Fu, Phonon properties and thermal conductivity from first principles, lattice dynamics, and the Boltzmann transport equation, J. Appl. Phys. **125**, 011101 (2019).
[16] A. Cepellotti and N. Marzari, Thermal Transport in Crystals as a Kinetic Theory of Relaxons, Phys. Rev. X **6**, 041013 (2016).
[17] A. Cepellotti and N. Marzari, Transport waves as crystal excitations, Phys. Rev. Materials **1**, 045406 (2017).
[18] G. Fugallo, M. Lazzeri, L. Paulatto, and F. Mauri, *Ab initio* variational approach for evaluating lattice thermal conductivity, Phys. Rev. B **88**, 045430 (2013).
[19] G. Fugallo, A. Cepellotti, L. Paulatto, M. Lazzeri, N. Marzari, and F. Mauri, Thermal conductivity of graphene and graphite: Collective excitations and mean free paths, Nano Lett. **14**, 6109 (2014).
[20] W. Li, J. Carrete, N. A. Katcho, and N. Mingo, ShengBTE: A solver of the Boltzmann transport equation for phonons, Comput. Phys. Commun. **185**, 1747 (2014).
[21] A. Chernatynskiy and S. R. Phillpot, Phonon transport simulator (PhonTS), Comput. Phys. Commun. **192**, 196 (2015).
[22] J. Carrete, B. Vermeersch, A. Katre, A. van Roekeghem, T. Wang, G. K. H. Madsen, and N. Mingo, almaBTE: A solver of the space–time dependent Boltzmann transport equation for phonons in structured materials, Comput. Phys. Commun. **220**, 351 (2017).
[23] C. Hua and A. J. Minnich, Analytical Green's function of the multidimensional frequency-dependent phonon Boltzmann equation, Phys. Rev. B **90**, 214306 (2014).
[24] L. Zeng and G. Chen, Disparate quasiballistic heat conduction regimes from periodic heat sources on a substrate, J. Appl. Phys. **116**, 064307 (2014).
[25] K. C. Collins, A. A. Maznev, Z. Tian, K. Esfarjani, K. A. Nelson, and G. Chen, Non-diffusive relaxation of a transient thermal grating analyzed with the Boltzmann transport equation, J. Appl. Phys. **114**, 104302 (2013).
[26] P. B. Allen, Analysis of nonlocal phonon thermal conductivity simulations showing the ballistic to diffusive crossover, Phys. Rev. B **97**, 134307 (2018).
[27] V. Chiloyan, S. Huberman, Z. Ding, J. Mendoza, A. A. Maznev, K. A. Nelson, and G. Chen, Green's functions of the Boltzmann transport equation with the full scattering matrix for phonon nanoscale transport beyond the relaxation-time approximation, Phys. Rev. B **104**, 245424 (2021).
[28] A. A. Balandin, S. Ghosh, W. Bao, I. Calizo, D. Teweldebrhan, F. Miao, and C. N. Lau, Superior thermal conductivity of single-layer graphene, Nano Lett. **8**, 902 (2008).
[29] S. Chen, A. L. Moore, W. Cai, J. W. Suk, J. An, C. Mishra, C. Amos, C. W. Magnuson, J. Kang, L. Shi, and R. S. Ruoff, Raman measurements of thermal transport in suspended monolayer graphene of variable sizes in vacuum and gaseous environments, ACS Nano **5**, 321 (2011).
[30] F. Libbi, N. Bonini, and N. Marzari, Thermomechanical properties of honeycomb lattices from internal-coordinates potentials:

The case of graphene and hexagonal boron nitride, 2D Mater. **8**, 015026 (2021).

[31] N. Bonini, J. Garg, and N. Marzari, Acoustic phonon lifetimes and thermal transport in free-standing and strained graphene, Nano Lett. **12**, 2673 (2012).

[32] In the simulations, we use $N_q = 120 \times 120q$ points to sample the Brillouin zone of graphene, and for δ functions in Eq. (10) we use the Gaussian broadening function $\delta(x) = \exp -(x/\sigma)^2/\sqrt{\pi}\sigma$, with $\hbar\sigma = 0.9$ meV.

[33] C. Hua and A. J. Minnich, Heat dissipation in the quasiballistic regime studied using the Boltzmann equation in the spatial frequency domain, Phys. Rev. B **97**, 014307 (2018).

[34] V. Chiloyan, S. Huberman, A. A. Maznev, K. A. Nelson, and G. Chen, Thermal transport exceeding bulk heat conduction due to nonthermal micro/nanoscale phonon populations, Appl. Phys. Lett. **116**, 163102 (2020).

[35] B. Vermeersch and A. Shakouri, Nonlocality in microscale heat conduction, arXiv:1412.6555.

[36] B. Vermeersch, J. Carrete, N. Mingo, and A. Shakouri, Superdiffusive heat conduction in semiconductor alloys. I. Theoretical foundations, Phys. Rev. B **91**, 085202 (2015).

[37] P. B. Allen and N. A. Nghiem, Nonlocal phonon heat transport seen in 1-d pulses Phys. Rev. B **105**, 174302 (2022).

[38] X. Li and S. Lee, Crossover of ballistic, hydrodynamic, and diffusive phonon transport in suspended graphene, Phys. Rev. B **99**, 085202 (2019).

[39] L. Lindsay and D. A. Broido, Optimized Tersoff and Brenner empirical potential parameters for lattice dynamics and phonon thermal transport in carbon nanotubes and graphene, Phys. Rev. B **81**, 205441 (2010).

[40] X. Gu, Z. Fan, H. Bao, and C. Y. Zhao, Revisiting phonon-phonon scattering in single-layer graphene, Phys. Rev. B **100**, 064306 (2019).

[41] V. Perebeinos and J. Tersoff, Valence force model for phonons in graphene and carbon nanotubes, Phys. Rev. B **79**, 241409(R) (2009).

[42] J. A. Johnson, A. A. Maznev, J. Cuffe, J. K. Eliason, A. J. Minnich, T. Kehoe, C. M. S. Torres, G. Chen, and K. A. Nelson, Direct Measurement of Room-Temperature Nondiffusive Thermal Transport Over Micron Distances in a Silicon Membrane, Phys. Rev. Lett. **110**, 025901 (2013).

[43] L. Zeng, K. C. Collins, Y. Hu, M. N. Luckyanova, A. A. Maznev, S. Huberman, V. Chiloyan, J. Zhou, X. Huang, K. A. Nelson *et al.*, Measuring phonon mean free path distributions by probing quasiballistic phonon transport in grating nanostructures, Sci. Rep. **5**, 17131 (2015).

[44] Z. Li, S. Xiong, C. Sievers, Y. Hu, Z. Fan, N. Wei, H. Bao, S. Chen, D. Donadio, and T. Ala-Nissila, Influence of thermostatting on nonequilibrium molecular dynamics simulations of heat conduction in solids, J. Chem. Phys. **151**, 234105 (2019).

[45] D. G. Cahill, Analysis of heat flow in layered structures for time-domain thermoreflectance, Rev. Sci. Instrum. **75**, 5119 (2004).

[46] K. M. Hoogeboom-Pot, J. N. Hernandez-Charpak, X. Gu, T. D. Frazer, E. H. Anderson, W. Chao, R. W. Falcone, R. Yang, M. M. Murnane, H. C. Kapteyn, and D. Nardi, A new regime of nanoscale thermal transport: Collective diffusion increases dissipation efficiency, Proc. Natl. Acad. Sci. USA **112**, 4846 (2015).

[47] M. Lundstrom, *Fundamentals of Carrier Transport*, 2nd ed. (Cambridge University Press, Cambridge, 2000).

[48] Center for Computational Research, University at Buffalo, http://hdl.handle.net/10477/79221.